https://doi.org/10.5194/egusphere-2025-3648
Preprint. Discussion started: 12 December 2025

Multi-coupling analysis of temperate glacier stability: A case study of Midui glacier on Tibet, China

Guang Li [1, 2], Minggao Tang [1, 2 *], Huanle Zhao [1, 2], Daojing Guo [1, 2], Xiaonan Yang [1, 2], Xu Ran [1, 2]

[1] State Key Laboratory of Geohazard Prevention and Geoenvironment Protection, Chengdu University of Technology, Chengdu 610059, China

[2] College of Environment and Civil Engineering, Chengdu University of Technology, Chengdu 610059, China

[*] Correspondence to: Minggao Tang (tmg@cdut.edu.cn)

Abstract： Temperate glaciers are particularly sensitive to climate warming. The instability of temperate glaciers and their geohazards chains threaten the safety of residents and engineering facilities. However, limited attention has been paid to the quantitative assessment of the stability of temperate glaciers, and the response of dynamic characteristics and hydrothermal distribution to climate change is still unclear. Herein, based on thermo-hydromechanical numerical simulation, the dynamic characteristics and hydrothermal variation of temperate glaciers are analyzed, and a conceptual model for quantitative evaluation of the stability and potential collapse area is proposed. The results show that: (1) The low temperature area is mainly concentrated in the glacier upper reaches. The minimum temperature of the glacier in the cold and warm season can reach -10 and -8 ℃, respectively, and the basal temperature is maintained at melting point temperature. (2) The maximum flow velocity in the cold and warm seasons are 45 and 50 m/yr, respectively. The maximum flow velocity is concentrated in the area with the largest glacier thickness. (3) The glacier instability strip is located in the glacier upper reaches. During the year, the factor of safety reached a maximum of 2.03 in February and a minimum of 1.48 in August.

1. Introduction

Glaciers are considered to be indicators of climate change. Temperate glaciers at low latitudes are particularly sensitive to climate change (Li et al., 2008). According to the Blue Book on Climate Change in China 2023, the global warming trend has progressed. From 1901 to 2022, the average surface temperature in China increased by 0.16 ℃ every decade (China Meteorological Administration Climate

https://doi.org/10.5194/egusphere-2025-3648
Preprint. Discussion started: 12 December 2025

Change Center, 2023). As Asian water tower, the Tibetan Plateau (TP) has the fastest warming rate. Rising temperatures have accelerated the melting and flow of mountain glaciers, leading to glacier instability (Jacquemart et al., 2020). The hydrothermal changes and stability of glaciers have a profound impact on the regional natural environment and social economy. The TP has become a hot spot for studying climate and glacier changes (Wang et al., 2019).

In recent years, the glacial and periglacial environment is experiencing an increase in geohazards due to cryosphere change (Faillettaz et al., 2015; Gilbert et al., 2015). The ice avalanches (IAs) caused by glacier instability on the TP have increased. The sudden instability and geohazard chains of glaciers will pose a serious threat to the safety of residents and engineering facilities downstream (Zhang et al., 2023b). In 2016, two giant IAs occurred in the Ngari, Tibet, with a volume of 68×10^6 m^3 and 83×10^6 m^3, respectively, resulting in the deaths of 9 herdsmen and hundreds of livestock (Kääb et al., 2018). In 2018, the Sedongpu IA in southeastern Tibet caused an IA-debris flow-dammed lake (Li et al., 2022; Li et al., 2024). There have been four IAs in Anyemaqen Mountains, Qinghai Province since 2004, destroying large grasslands and affecting 732 herders (Zou et al., 2023; Zhang et al., 2023a).

Remote sensing images can observe glacier flow processes and area changes (Garg et al., 2019; Millan et al., 2022; Altena et al., 2019). However, the lack of data in some remote sensing images will affect the monitoring accuracy and resolution of time series (Cook et al., 2023). Glacier numerical simulation has become the best method to analyze the dynamic process (Zhen et al., 2016). Through two-dimensional and three-dimensional thermo-dynamic coupling models, the changes in the velocity and stress field of the glacier are obtained to reveal the response mechanism to climate change (Zhang et al., 2013; Wang et al., 2018; Zhao et al., 2013). The Full Stokes flow laws that comply with the mass and momentum conservation is used to systematically describe the movement of glaciers. It can be combined with shallow ice approximate model, shallow ice shelf approximate model, and high-order approximate model. They are applied to the finite element numerical simulation, which can not only obtain the velocity field of the glacier, but also the thermodynamic state (Zhao et al., 2022; Karlsson et al., 2021; Ai et al., 2019). Based on the Full Stokes model, Seddik et al. (2019) studied the force balance state of the Bowdoin glacier, and explained the influence of base lubrication and tide on the glacier stability. Gong et al. (2017) evaluated the importance of basal boundary conditions in surging glacier transient

https://doi.org/10.5194/egusphere-2025-3648
Preprint. Discussion started: 12 December 2025

simulations. Glacier numerical simulations have been extensively studied. Due to the complex thermo-hydromechanical coupling physical process of temperate glaciers, the fine simulation research on temperate glaciers in southeastern Tibet is still scarce, especially the flow velocity, temperature, heat flux, and stress analysis of glaciers under rising temperature. The stability of temperate glaciers is closely related to thermodynamic processes. The research gap limits the accurate assessment of glacier stability.

Rising temperatures reduce the viscosity and shear strength of ice, and the increase of glacier flow velocity makes the ice more prone to brittle fracture, thus inducing glacier instability. When the basal fluid pressure at the ice-rock interface reaches a critical value, rapid sliding of the glacier will lead to IAs. Regional differences in glacier change indicate that factors such as bedrock topography, elevation distribution, subglacial meltwater, and moraine cover lead to different of the internal and external dynamic coupling modes (Vallot et al., 2017; Jiskoot et al., 2017). Atmospheric temperature, rainfall, and geological tectonic activity are key factors in studying the mechanism of glacier instability (Tang et al., 2024). Faillettaz et al. (2015) pointed out that temperate glacier instability usually occurs when the slope is about 30°. The rupture location occurs within the ice, on the bedrock, and in the bedrock in temperate regions. Gilbert et al. (2016) analyzed the thermal status, basal friction and shear stress before the Aru IAs, but did not quantitatively evaluate the glacier stability. Glacier instability often occurs at the glacier scarp or periglacial region, and it is of great significance to clarify the stability changes and potential collapse zone (Kääb et al., 2024).

Most mountain glaciers in low-altitude areas are temperate glaciers. The response of temperate glacier dynamics and stability to climate change can provide some insights into the instability mechanism. Herein, the Midui glacier is taken as an example. Based on the glacier thickness and meteorological data, considering the multi-physical processes in the glacier flow, a thermo-hydromechanical coupling numerical model is established to analyze the dynamic characteristics and hydrothermal changes of glaciers under climate warming, and the glacier stability and potential collapse zone are evaluated.

2. Study area

The Midui glacier is located in Midui valley, Bomi County, Tibet (Fig. 1), and it is a typical low-altitude temperate glacier. The Midui glacier presents an obvious firn basin, forming a very steep back

https://doi.org/10.5194/egusphere-2025-3648
Preprint. Discussion started: 12 December 2025

wall (Fig. 2a). The glacier fall is located under the firn basin, and it is at an altitude of 4850~4100 m. The glacier tongue of Midui glacier is directly connected to the glacial lake (Fig. 2b), and the collapsed glacier directly falls into the glacial lake (Fig. 2c).

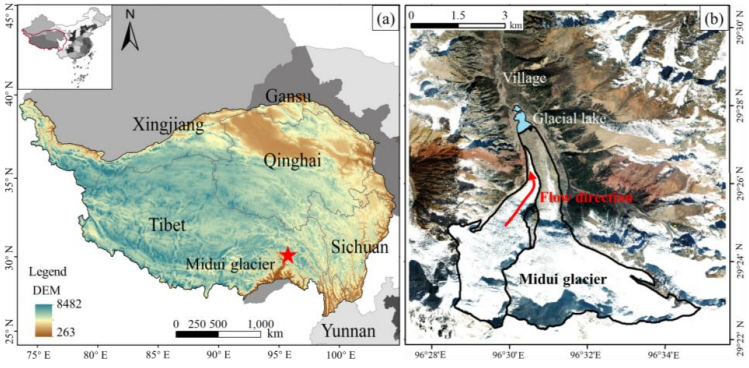

Figure 1. Geographical location of study area. (a) The Tibetan Plateau. (b) The Midui glacier.

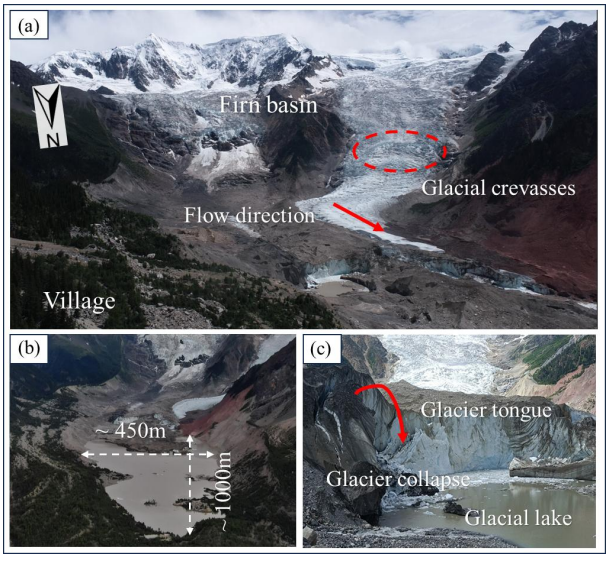

Figure 2. General introduction of study area. (a) The overview of study area. (b) The glacial lake. (c) The intersection of Midui glacier and glacial lake.

The Glacier tongue is covered by moraine with a thickness of 50 ~ 80 cm (Fig. 3a and b). The main lithologies are granite and limestone. There are many longitudinal and horizontal crevasses on the glacier surface (Fig. 3c and d). The crevasses can be up to tens of meters long. The longitudinal crevasses are usually wedge-shaped. The upper width is usually greater than 0.7 m, and the lower width is narrower.

https://doi.org/10.5194/egusphere-2025-3648
Preprint. Discussion started: 12 December 2025

It penetrates into glacier for several meters. Meltwater seeps into the glacier along crevasses and recharges the glacial lake. There will be large rocks on the glacier surface. Compared with bare ice, the melting rate of ice under large rocks is significantly reduced, resulting in the formation of glacial tables, which are usually composed of a rock supported by narrow ice legs (Fig. 3e and f).

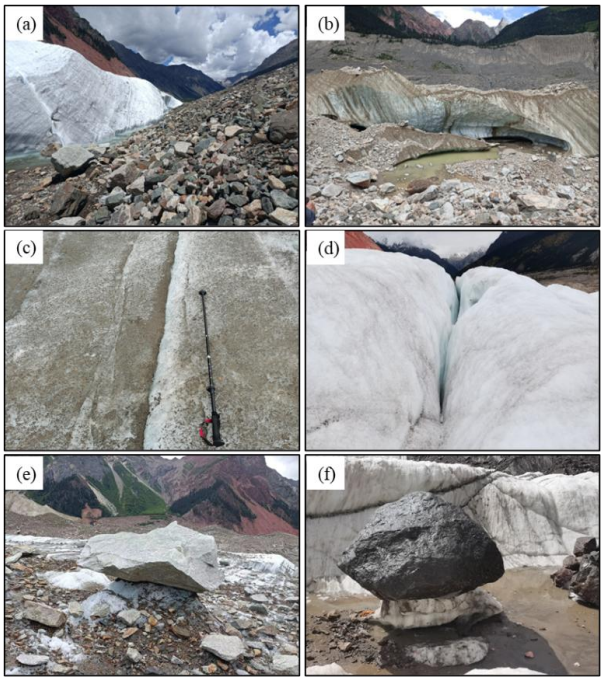

Figure 3. Geological phenomena during the flow of temperate glacier. (a) and (b) are glacial tills. (c) and (d) are glacial crevasses. (e) and (f) are glacial tables.

On July 15, 1988, there was an IA in the study area. For meteorological-driven geohazards, the meteorological data sets of 1 day (the day of the triggering), 7 days (6 days prior the triggering), 30 days (29 days prior the triggering), and 90 days (89 days prior the triggering) can be analyzed to understand the relationship between meteorological anomalies and geohazards (Paranunzio et al., 2024). Therefore, we selected the average, minimum, and maximum temperatures (T_{mean}, T_{min}, and T_{max}) from April 17,1988 to July 15,1988 and the total precipitation (including rain and snowfall) from 1980 to 1988, as shown in Fig. 4 (The data were acquired from Free Weather API: https://open-meteo.com/). There were three wet years from 1980 to 1988: 1984, 1985 and 1988. The highest precipitation in 1988 (the year of the triggering) was 2448.9 mm, which was 607.4 mm higher than that in 1987. In June 1988, the highest

https://doi.org/10.5194/egusphere-2025-3648
Preprint. Discussion started: 12 December 2025

temperature reached 30.1 ℃, close to the instantaneous maximum temperature for many years. In July 1988, the high temperature lasted for many days before IA, and the daily average temperature reached 7.6 ℃ ~ 11.6 ℃. The abnormally warm and humid climate caused a large amount of meltwater to seep into the glacier base. The buoyancy and seepage pressure of the glacier tongue increased, and the frictional resistance of the glacier base decreased, resulting in an IA with a scale of 3.6×10^5 m^3 (Dang et al., 2019). The disintegrated glacier poured into the glacial lake to form glacier lake outburst floods (GLOFs).

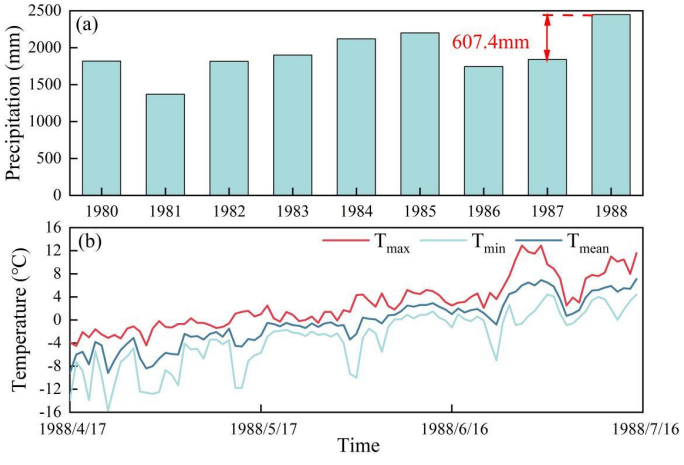

Figure 4. Historical climate analysis. (a) The total precipitation (including rain and snowfall). (b) The average, minimum, and maximum temperatures.

3. Methods

3.1. Mathematical model

There have been serious IA and geohazard chain in the study area. In order to explore the impact of climate change on glacier stability and temperature field, a conceptual model was used to describe it (Fig. 5). The momentum and continuity equations and incompressible heat equations have been used to describe the ice velocity, ice temperature, and stress distribution. Subglacial water flow occurs within the permeable layer and is considered as unsaturated seepage, which is described by the Richards equation. The specific equation descriptions are as follows.

https://doi.org/10.5194/egusphere-2025-3648
Preprint. Discussion started: 12 December 2025

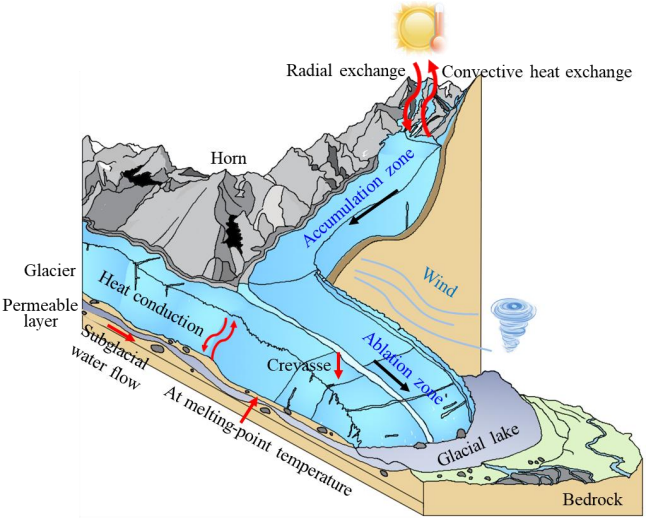

Figure 5. A conceptual model akin to the Midui glacier.

3.1.1. The temperature equation

Glacier flow controls the basic process of ice material deformation and energy budget. The temperature distribution of glacier can be calculated by energy balance equation (Tannehill et al., 1997).

$$\rho c_p \frac{\partial T}{\partial t} + \rho c_p u \bullet \nabla T = Q + \nabla (k \bullet \nabla T) \quad (1)$$

Here, c_p is the heat capacity; T is the temperature; u is the velocity vector; Q is the heat source term; and k is the thermal conductivity of ice. The heat capacity and thermal conductivity of ice change with temperature (Ritz, 1987), expressed as:

$$c_p(T) = 146.3 + 7.253T \quad (2)$$

$$k(T) = 9.828e^{-0.0057T} \quad (3)$$

Herein, the heat source term considered the convective heat exchange (q_c) and radiative heat exchange (q_r) between the ambient temperature and the glacier surface. The convective heat exchange uses forced convective heat flux (Incropera et al., 2007):

$$-n \bullet q_c = h(T_{ext} - T) \quad (4)$$

https://doi.org/10.5194/egusphere-2025-3648
Preprint. Discussion started: 12 December 2025

$$h = \begin{cases} 2\frac{K_{ext}}{L}\frac{0.3387\,\mathrm{Pr}^{1/3}\bullet\mathrm{Re}^{1/2}}{\left[1+\left(\frac{0.0468}{\mathrm{Pr}}\right)^{2/3}\right]^{1/4}} & \mathrm{Re} \le 5\times10^{5} \\ 2\frac{K_{ext}}{L}\mathrm{Pr}^{1/3}\left(0.037\,\mathrm{Re}^{4/5}-871\right) & \mathrm{Re} > 5\times10^{5} \end{cases} \quad (5)$$

Here, n is the outward unit normal vector; h is the convective heat transfer coefficient; T_{ext} is the ambient temperature; L is the characteristic length; K_{ext} is the air heat transfer coefficient; Pr is the Prandtl number.

Radiative heat transfer is based on the Stefan-Boltzmann law:

$$-\mathrm{n}\bullet q_r = \sigma\varepsilon_s\left(T_{ext}^4 - T^4\right) \quad (6)$$

Here, σ is the Stefan-Boltzmann constant; ε_s is the land surface emissivity.

The temperature of the bedrock can be assumed to be the melting point temperature (Wagner et al., 1994):

$$T = T_{tp} - b_{CC}(p - p_{tp}) \quad (7)$$

Here, T_{tp} is the melting point temperature of water; p_{tp} is the standard atmospheric pressure; β_{CC} is the Clausius-Clapeyron constant.

3.1.2. Subglacial water flow

There is a large amount of meltwater at the temperate glacier base. The subglacial water flow plays a role in transporting the fine particles produced by the glacier erosion. The water flow is accompanied by a large number of debris and soil to form unsaturated seepage, which is described by Richards equation (Richard, 1931):

$$\rho\left(\frac{C_{\mathrm{m}}}{\rho g}+S_{\mathrm{e}}S\right)\frac{\partial P}{\partial \mathrm{t}}+\nabla\rho\left(-\frac{K_s}{\mu}K_r(\nabla P+\rho\mathrm{g}\nabla D)\right)=Q_m \quad (8)$$

Here, C_m is the bulk density of water; ρ is the water density; S_e is the effective saturation: $S_e=\frac{(\theta-\theta_r)}{\theta_s-\theta_r}$; θ, θ_s, and θ_r are the water content, saturated water content, and residual water content,

https://doi.org/10.5194/egusphere-2025-3648
Preprint. Discussion started: 12 December 2025

respectively; S is the storativity; P is the pressure; K_s is the saturated hydraulic conductivity; μ is the fluid viscosity; K_r is the relative permeability; D is the position head; Q_m is the source item.

When the soil-water characteristic curve, the relationship between soil moisture content and permeability coefficient, and the corresponding initial values and boundary conditions are known, the unsaturated seepage problem can be analyzed based on the Richards equation. The van Genuchten model is used to describe the hydraulic characteristics of the subglacial permeable layer (Van, 1980).

$$h = -(S_e^{\frac{1}{-m}} - 1)^{\frac{1}{n}} / \alpha \tag{9}$$

$$S_e = \frac{\theta_l - \theta_r}{\theta_s - \theta_r} = \begin{cases} \dfrac{1}{\left[1 + |\alpha h|^n\right]^m} & h < 0 \\ 1 & h \geq 0 \end{cases} \tag{10}$$

The relationship between pressure head and liquid water content is obtained by combining the above equations:

$$h = -\left[\left(\frac{\theta_l - \theta_r}{\theta_s - \theta_r}\right)^{\frac{1}{-m}} - 1\right]^{\frac{1}{n}} / \alpha \tag{11}$$

$$K = \begin{cases} K_s S_e^{l}\left[1 - (1 - S_e^{\frac{1}{m}})^m\right]^2 & h < 0 \\ K_s & h \geq 0 \end{cases} \tag{12}$$

Here, h is the pressure head; m, n, and l are empirical parameters, and $m = 1 - \frac{1}{n}$; α is the the reciprocal of soil air entry value; θ_l is the liquid water content; K_s is the saturated hydraulic conductivity; K is the hydraulic conductivity.

3.1.3. The velocity equation

Motion is the inherent natural property of glaciers. As an incompressible non-Newtonian fluid, the motion equation of glacier can be expressed by Stokes equation, which can reflect the basic mechanical law of viscous fluid flow and satisfy the conservation of momentum (Tannehill et al., 1997):

$$\rho_i \frac{\partial \mathrm{u}}{\partial t} = \nabla \bullet [-pI + \mu(\nabla u^T)] + \rho_i g \tag{13}$$

https://doi.org/10.5194/egusphere-2025-3648
Preprint. Discussion started: 12 December 2025

$$\nabla \bullet u = 0 \tag{14}$$

Here, ρ is the ice density; u is the velocity vector; p is the pressure; g is the acceleration of gravity; μ is the dynamic viscosity.

Ice shows a change in viscosity when it is sheared. The relationship between shear strain rate and shear stress of ice can be expressed by Glenn flow law (Glen, 1955):

$$\mu = \frac{1}{2} A^{-\frac{1}{n}} \bullet \gamma^{n-1} \tag{15}$$

Here, γ is the shear rate, which can be defined as the strain rate tensor modulus: $\gamma(u) = \left\| \frac{1}{2}\left(\nabla u + \nabla u^{T}\right) \right\|$; n is the flow characteristic index of ice; A is the flow rate factor.

To fully define the Glenn flow law, it is also necessary to define the consistency index of ice:

$$m = \frac{1}{2} A^{-\frac{1}{n}} \tag{16}$$

Here, m is the consistency index of ice.

The viscosity of ice depends not only on the shear rate, but also on temperature and pressure. The Arrhenius law is used to represent the flow rate factor, which is the expression of temperature (T) and pressure (p) (Stocker et al., 2013):

$$A(T, p) = A_0 e^{\left(\frac{-Q}{RT}\right)} \tag{17}$$

Here, A_0 is the flow rate constant, and the expression is $A_0 = \begin{cases} 3.985e^{-13} & T \le -10℃ \\ 1.916e^{3} & T > -10℃ \end{cases}$; Q is the activation energy, and the expression is $Q = \begin{cases} 60e^{3} & T \le -10℃ \\ 139e^{3} & T > -10℃ \end{cases}$; R is the Stefan-Boltzman.

3.1.4. Mechanical equations

There are shear fracture surfaces caused by crevasses before the glacier instability, which will cause rapid disintegration and collapse of glacier under gravity. The strength reduction method has been proved to be reasonable for predicting the glaciers stability lacking large displacement precursor information (Wei et al., 2024). Therefore, elastic-plastic constitutive equation and strength reduction method were used to study the glacier stability. The glacier stability can be considered as a mechanical problem

https://doi.org/10.5194/egusphere-2025-3648
Preprint. Discussion started: 12 December 2025

involving matrix failure. The quantitative evaluation of glacier stability can refer to the slope stability evaluation method, and the elastic-plastic analysis adopts Mohr-Coulomb criterion. The Mohr-Coulomb yield function and the related plastic potential are:

$$F = Q = \mathrm{m}(\theta)\sqrt{J_2} + \alpha I_1 - k \tag{18}$$

$$\mathrm{m}(\theta) = \sqrt{\frac{1}{3}}\left((1+\sin\varphi)\cos\theta - (1-\sin\varphi) * \cos\left(\theta + \frac{2\pi}{3}\right)\right) \tag{19}$$

$$\alpha = \frac{\sin\varphi}{3} \tag{20}$$

$$k = c \cdot \cos\varphi \tag{21}$$

Here, θ is the Lode angle; J_2 is the second invariant of deviatoric stress tensor; I_1 is the first invariant of stress tensor; c is the cohesion; φ is the internal friction angle.

The cohesion and internal friction angle of glacier ice are set as a quadratic function related to temperature. The function is obtained by the author 's laboratory test (Tang et al., 2023). Their relationships with temperature are as follows:

$$\mathrm{c} = 155.04 - 1.49T - 0.02T^2 \tag{22}$$

$$\varphi = 1.91 - 1.23T - 0.02T^2 \tag{23}$$

The strength reduction method can reflect the instability process of glaciers after strength degradation. This method is to reduce the shear strength parameters in equal proportion until the glacier reaches the limit equilibrium state. The reduction coefficient at this time is the factor of safety (FOS):

$$c' = \frac{c}{FOS} \tag{24}$$

$$\varphi' = \arctan\left(\frac{\tan\varphi}{FOS}\right) \tag{25}$$

Here, FOS is the reduction coefficient; c' and φ' are the reduced cohesion and internal friction angle, respectively.

3.2. Computational model and parameters

(1) Numerical model

In order to analyze the velocity, temperature and stress distribution of the Midui glacier, a two-dimensional numerical simulation was established. Firstly, the section line is drawn based on the

https://doi.org/10.5194/egusphere-2025-3648
Preprint. Discussion started: 12 December 2025

centerline of the glacier movement (Fig. 6a). As shown in Fig. 6b and c, the topography of the surface and base is obtained from the surface elevation and ice thickness data (The DEM data were acquired from: https://earthexplorer.usgs.gov/, and the glacier thickness were acquired from: https://www.research-collection.ethz.ch/handle/20.500.11850/315707). The base topography is the surface elevation minus the ice thickness. Finally, the two-dimensional cross-section of the Midui glacier is obtained (Fig. 6d). The length of the glacier computational domain is 874.7 m, and the altitude difference is 730 m. The thickest of glacier reaches 77.9 m, and the thinnest is 9.37 m. The thickness of the subglacial water flow permeability layer was assumed to be 1 m.

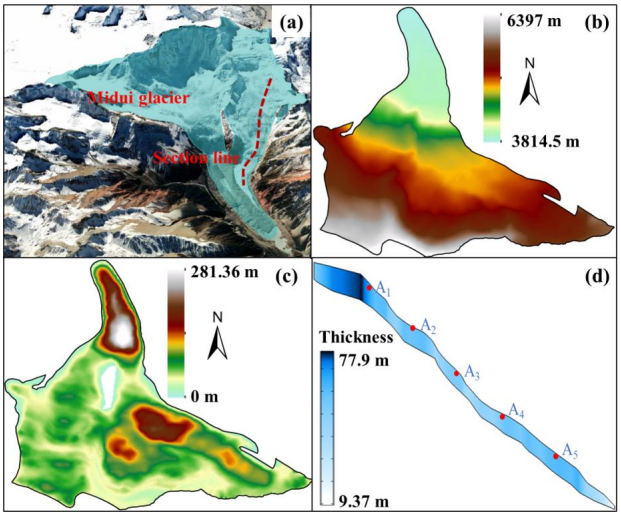

Figure 6. Computational model for glacier. (a) Longitudinal section diagram. (b) Glacier DEM. (c) Glacier thicknes. (d) The 2D section of computational model.

(2) Boundary conditions and parameter

For heat transfer, the glacier base is set to the melting point temperature. The left and right boundaries are set as free boundaries, and the heat flux can enter and leave the domain. The glacier surface undergoes convective heat exchange and radiative heat exchange with the atmospheric environment, where the wind speed is set to the average value of 1.01 m/s over the past 20 years. The transient temperature field boundary condition of the glacier surface adopts the Dirichlet boundary, which is obtained by directly giving the boundary temperature value, that is, a variable about space and time is known:

https://doi.org/10.5194/egusphere-2025-3648
Preprint. Discussion started: 12 December 2025

$$T = T(x, y, t) \tag{26}$$

Here, we use the boundary layer theory to fit the long-term observed atmospheric temperature function with the temperature increment. The empirical formula of glacier surface temperature change can be obtained.

The seepage field is used to analyze the subglacial permeable layer. The left of the permeable layer is a symmetrical boundary with a certain height of water head. The bottom is an impervious boundary, the right is a seepage boundary, and the top is a non-flow boundary.

For the velocity field, the basal temperature is at the melting temperature, and the glacier can slide through the bottom. The ice-rock interface is set to the viscous slip boundary condition. The glacier surface is a stress-free boundary. The left and right boundaries are normal constraints. The left boundary exerts pressure on the glacier, thereby accelerating the glacier flow, and the right boundary generates resistance to the flow.

The force field is used for stability analysis of glaciers. First, the stress field of the model under gravity is calculated, and the stress is provided to the model as prestress for recalculation, thereby achieving stress balance and making the model have initial stress but no initial strain. The glacier surface and the right boundary are free boundary, the glacier base is a fixed constraint, and the left boundary is a horizontal constraint with vertical displacement freedom.

According to the references of the above formula, the parameters of each physical field in the calculation model are shown in Table 1.

Table 1. Model parameters

Parameter	Value (unit)	Description
ρ_i	910 (kg/m^3)	Density of ice
E	5.4×10^9 (Pa)	Young's modulus
ν	0.35	Poisson ratio
ε_s	0.97	Land surface emissivity
n	3	Flow characteristic index of ice
μ_i	5×10^{12} ($Pa\cdot s$)	Dynamic viscosity of ice
β_{CC}	9.8×10^{-8} (K/Pa)	Clausius-Clapeyron constant

https://doi.org/10.5194/egusphere-2025-3648
Preprint. Discussion started: 12 December 2025

T_{tp}	0.01 (℃)	Melting point temperature of water
p_{tp}	611.657 (Pa)	Standard atmospheric pressure
R	8.314 $J/(mol \cdot K)$	Universal gas constant
σ	$5.67 \times 10^{-8} [W/(m^2 \cdot k^4)]$	Stefan-Boltzmann constant
L	874.7 (m)	Characteristic length
θ_s	0.2 ($m^3 \cdot m^{-3}$)	Saturated water content
θ_r	0.05 ($m^3 \cdot m^{-3}$)	Residual water content
K_s	1.66×10^{-3} ($m \cdot s^{-1}$)	Saturated hydraulic conductivity
m	0.5	Van Genuchten model parameter
l	0.5	Van Genuchten model parameter
α	1 (m^{-1})	reciprocal of soil air entry value
T_m	-4.41 (℃)	Annual average temperature

4 Results

4.1 Model verification

In order to verify the reliability of the numerical coupling model and calculation method, we monitored the temperature at 1.2 meters below the glacier surface and glacier displacement in the study area (Fig. 7a, b). Field monitoring showed that the minimum temperature at 1.2 m below the ice surface was about-1.0 ℃, which occurred in mid-January. After 5 months, the glacier displacement reached 4.64 m. By comparing the observed values with simulated values (Fig. 7c, d), it can be found that they have the same change trend and good consistency. The root mean square error (RMSE) and mean absolute percentage error (MAPE) of temperature are 0.21 ℃ and 20.2%, respectively. The RMSE and MAPE of displacement are 0.14 m and 5.53%, respectively. Therefore, the model and numerical simulation results are basically reliable.

https://doi.org/10.5194/egusphere-2025-3648
Preprint. Discussion started: 12 December 2025

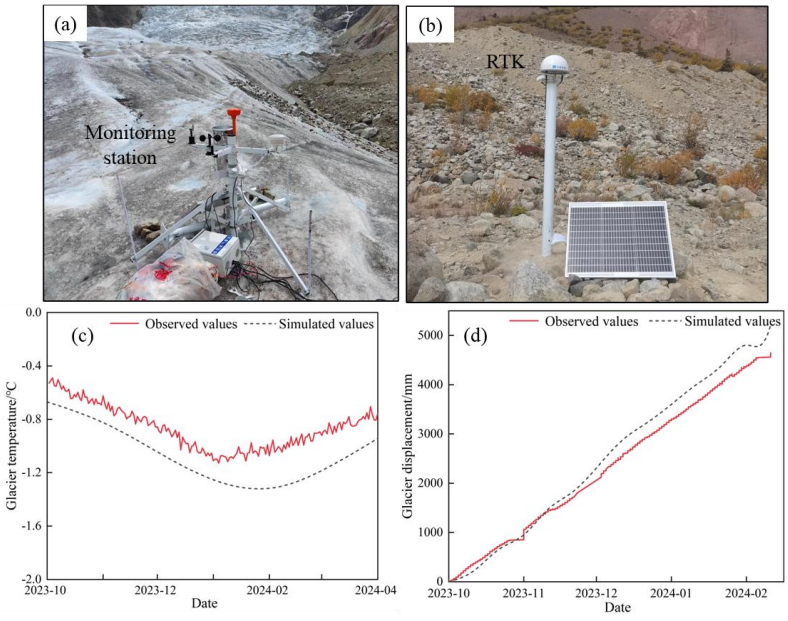

Figure 7. Comparison of observed and simulated values. (a) and (b) The monitoring station. (c) The glacier temperature. (d) The glacier displacement.

4.2 Glacier temperature field characteristic

Glacier temperature is controlled by surface and base temperatures and internal hydrothermal exchange processes, and it has a great influence on the glacier dynamics. Fig. 8 shows the glacier temperature distribution in cold and warm seasons. We observed that the glacier temperature in the cold season is significantly lower than that in the warm season, and the low temperature area is mainly concentrated in the glacier upper reaches. In the cold season, the minimum temperature reached -10 ℃, and the maximum temperature is lower than the ice melting temperature, indicating that the glacier is in material accumulation. The basal temperature is generally higher than the glacier surface temperature due to geothermal energy. In the warm season, the minimum temperature reached -8 ℃. At this time, the surface temperature is the highest, followed by the basal temperature, and the temperature in the glacier layer is the lowest. It indicates that the air temperature has the greatest contribution to the heat of the glacier.

https://doi.org/10.5194/egusphere-2025-3648
Preprint. Discussion started: 12 December 2025

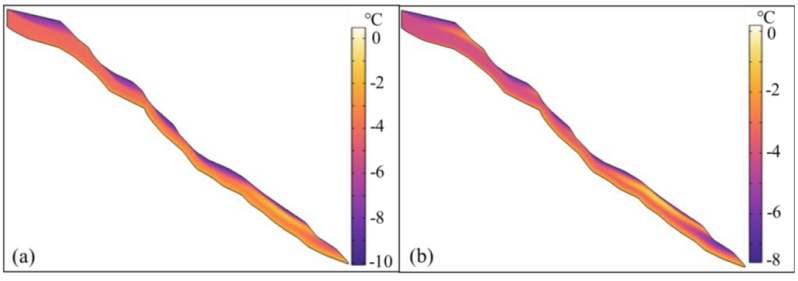

Figure 8. Glacier temperature distribution. (a) The cold season. (b) The warm season.

Fig. 9 shows the temperature variation of the glacier surface and base in January and July, respectively. It can be seen that the surface temperature is more sensitive to the external environment temperature. The glacier surface temperature varies greatly between January and July. The maximum fluctuation range is 9.1 ℃. There is almost no difference in the basal temperature between January and July, which is maintained at melting point temperature, and the fluctuation range is not more than 0.25 ℃. Seasonal temperature fluctuations on the glacier surface have little effect on the temperature of the glacier base, and the heat source is derived from the geothermal heat.

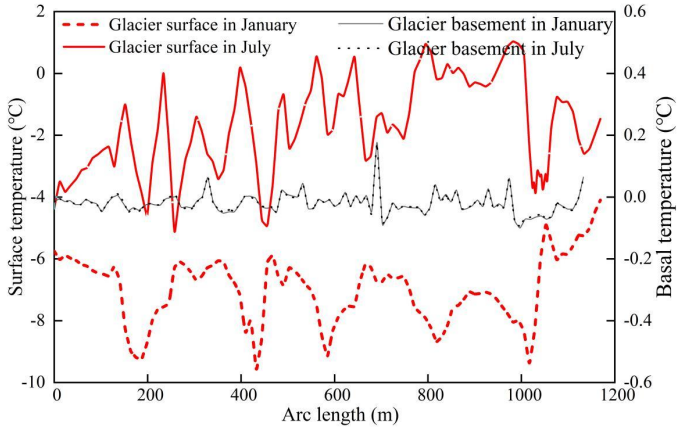

Figure 9. Glacier surface and base temperature changes.

The energy exchange between the glacier surface and the atmosphere affects the freezing and melting process, which can be further characterized by the heat flux. Fig. 10 is the heat flux change of the selected five points on the glacier surface in the past 10 years. The coordinate points are: A_1 (179.89, 4825.3), A_2 (321.95, 4699.5), A_3 (427.55, 4574.5), A_4 (568.5, 4449.8), and A_5 (726.02, 4325) (Fig. 6d). The positive heat flux indicates that the glacier surface is absorbing heat and melting. The negative heat

https://doi.org/10.5194/egusphere-2025-3648
Preprint. Discussion started: 12 December 2025

flux indicates that the glacier surface is exothermic and frozen, which is beneficial to the material balance of glaciers. It can be seen that the higher the glacier altitude, the greater the fluctuation range of heat flux. With the altitude increases, the air density decreases, and the rarefied air has lower efficiency in heat conduction and convection, so the heat is more likely to accumulate or dissipate quickly. At the same time, glaciers are often covered by snow at high altitudes, which increases the albedo of the sun and reduces the absorption of solar radiation. Due to the loss of long-wave radiation at night, the temperature difference between day and night increases and the fluctuation of heat flux increases.

During the year, the glacier surface absorbs more heat than it releases, indicating that the glacier material balance is in deficit and the glacier is retreating. In the first year, the heat flux was positive in late April, indicating that the glacier began to melt from late April, until October when the heat flux became negative and the glacier began to remain stable or thicken. By the 10th year, the glacier began to melt in early April. It shows that as the temperature rises over the years, the melting of the glacier will gradually increase. The material balance of the glacier is at a loss, and the loss will gradually increase.

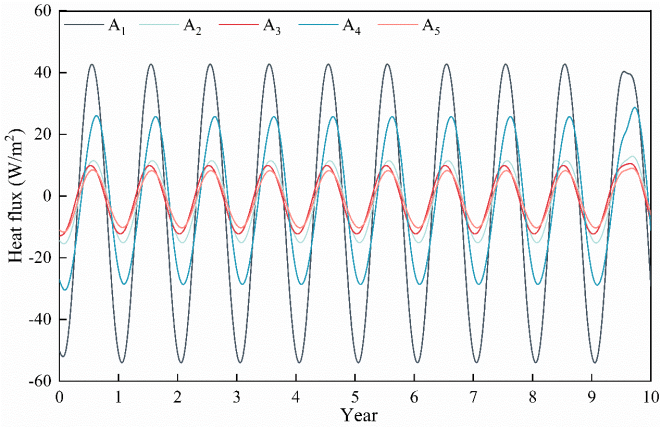

Figure 10. Glacier surface heat flux changes.

4.3 Glacier flow velocity and outward mass flow rate

Ice is a viscoelastic material that deforms under gravity. Its flow is determined by both the internal properties of the glacier and the external environment. Fig. 11 shows the flow velocity of glaciers in the cold and warm seasons after 10 years. The glacier velocity in the warm season is significantly greater than that in the cold season. The maximum flow velocity in the cold and warm seasons are 45 and 50

https://doi.org/10.5194/egusphere-2025-3648
Preprint. Discussion started: 12 December 2025

m/yr, respectively. Because it is a temperate glacier, there is water lubrication between the glacier and bedrock, and the base slides significantly. The maximum flow velocity is concentrated in the area with the largest glacier thickness. The thicker glaciers will produce greater basal pressure, increasing the rate of base sliding and glacier deformation.

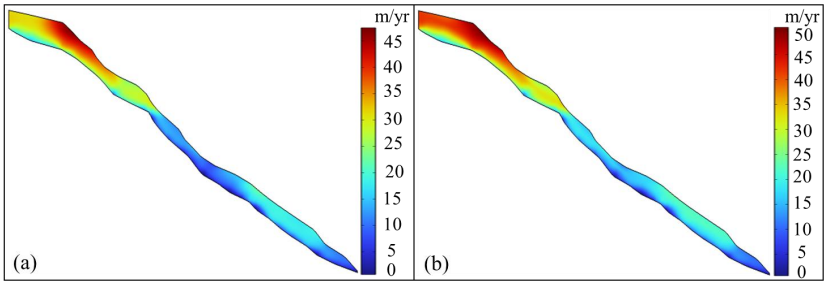

Figure 11. Glacier flow velocity distribution. (a) The cold season. (b) The warm season.

Mass flow rate is an important index to measure the mass balance of glaciers. The positive mass flow rate indicates that the glacier is melting. The outward mass flow rate of the glacier is controlled by glacier dynamics, physical properties, and environmental conditions. The variation trend of the outward mass flow rate of the glacier in 10 years is shown in Fig. 12. It can be seen that the mass flow rate increases year by year, and the growth rate suddenly increased in the sixth year, indicating that the glacier is melting more and more violently. In the 10th year, the outward mass flow reached 6.13×10^{-2} kg/s. The increase of outward mass flow accelerated the glacier flow, and glacier crevasses were generated. Glacier collapse and IA are more likely to occur, posing a threat to surrounding areas such as Midui village.

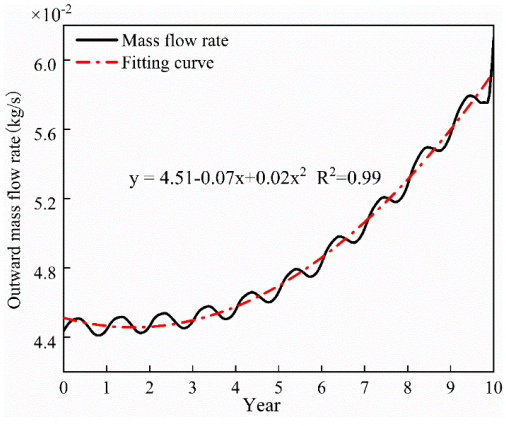

Figure 12. Outward mass flow rate of glacier.

https://doi.org/10.5194/egusphere-2025-3648
Preprint. Discussion started: 12 December 2025

4.4 Glacier stability analysis

Glacier stability analysis is to study the instability behavior and potential risk of IAs under different conditions. Herein, according to the thermo-hydromechanical coupling model and strength reduction method, the FOS of glacier can be obtained. Fig. 13 shows the relationship between the maximum displacement and the reduction coefficient of the glacier in January. At the beginning of the curve, the maximum displacement has remained at about 15 cm with the increase of reduction coefficient, and the displacement is small. When the reduction coefficient increases from 1.96 to 1.97, the maximum displacement in the glacier changes abruptly, increasing to nearly 1400 cm, and the curve has an obvious inflection point. Therefore, the FOS is preliminarily determined to be 1.96.

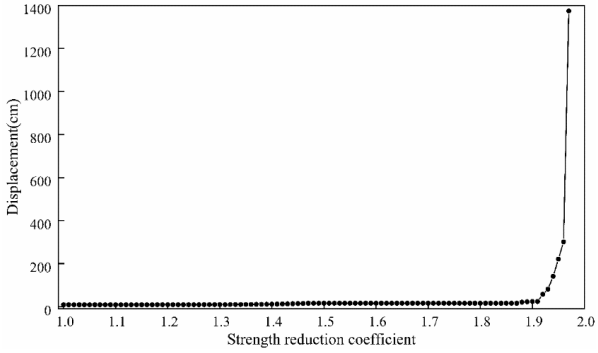

Figure 13. Variation of the glacier maximum displacement with reduction coefficient.

In order to further determine whether the glacier has reached the critical slip state when the reduction coefficient was 1.96, the plastic strain and the maximum shear strain were shown (Fig. 14). The maximum shear strain can be characterized by tresca stress, which refers to the difference between the maximum normal stress and the minimum normal stress. It can be seen that when the reduction coefficient is 1.96, the plastic zone at the glacier terminus has been completely penetrated and is arc-shaped. The maximum plastic strain is 3.1×10^{-3}. The tresca stress reaches the maximum value of 7.4×10^{5} N/m^2 at the same position, and the area with the highest shear stress is the most dangerous. According to the instability criterion, the FOS of glacier is 1.96.

https://doi.org/10.5194/egusphere-2025-3648
Preprint. Discussion started: 12 December 2025

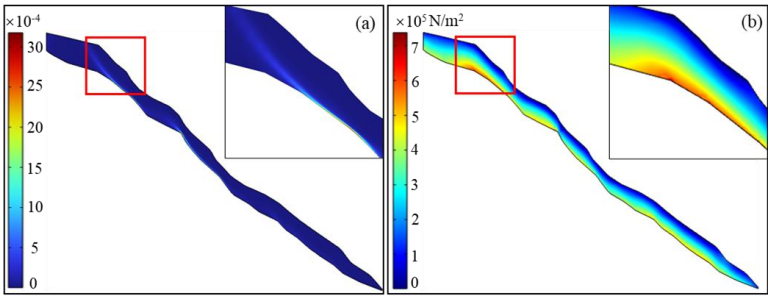

Figure 14. Plastic zone (a) and tresca stress (b) of glacier when the reduction coefficient is 1.96.

Fig. 15 shows the glacier displacement distribution when the reduction coefficient is 1.97. It can be seen that the glacier instability strip is mainly located in the glacier terminus. On the one hand, the slope on the glacier terminus is the steepest, and the distribution of crevasses is concentrated. Glacier is more prone to collapse. On the other hand, the glacier thickness in this region is the largest. The larger the thickness, the greater the basal pressure caused by gravity, which affects the basal sliding and glacier stability.

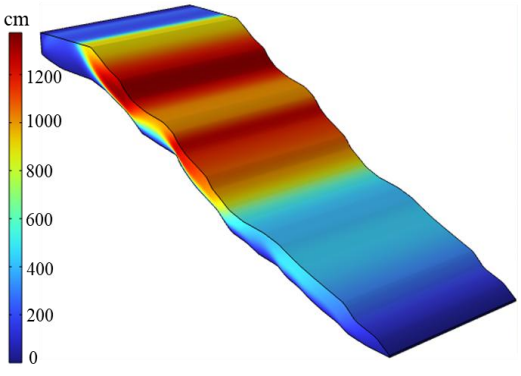

Figure 15. Glacier displacement when the reduction coefficient is 1.97.

Through the unsaturated seepage simulation of the permeable layer, the subglacial fluid pressure is obtained when the reduction coefficient is 1.96 (Fig. 16). The fluid pressure at the inlet and outlet of the glacier is low, and reaches the maximum in the upstream region. The high fluid pressure may cause the basal sliding, resulting in more prone to IA in this area. There are two peaks of fluid pressure in the process of decreasing, which is caused by the change of slope.

https://doi.org/10.5194/egusphere-2025-3648
Preprint. Discussion started: 12 December 2025

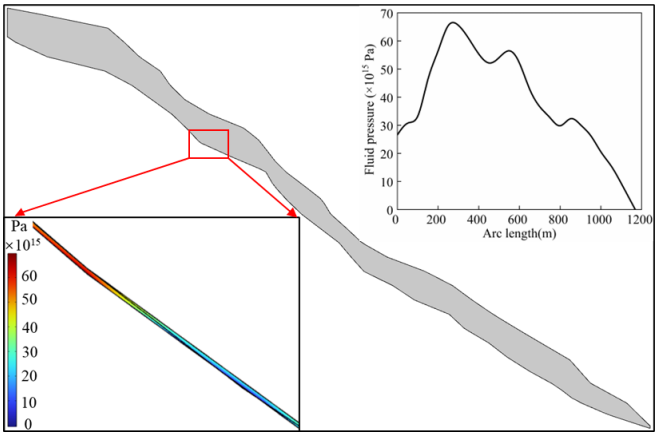

Figure 16. Subglacial fluid pressure.

In order to analyze the influence of monthly temperature change on glacier stability and maximum displacement, the monthly FOS and maximum displacement in the model are extracted (Fig. 17). With the change of monthly temperature, there is an obvious response relationship between FOS and maximum displacement. In the cold season, the FOS is large, the glacier stability is high, and the displacement of IA is also small. With the arrival of the warm season, rising temperatures reduce the glaciers stability and increase IA displacement. In February, the FOS reached a maximum value of 2.03, and the maximum displacement was only 1332 mm. The FOS decreased the most from May to July, and reached the minimum value of 1.48 in August. Since September, with the arrival of cold season, the FOS has gradually increased.

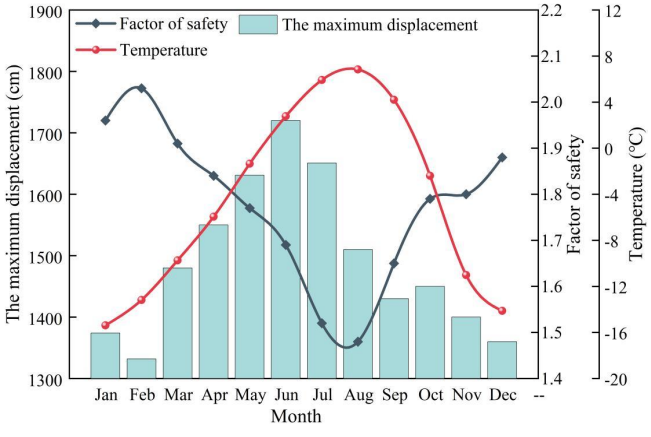

Figure 17. Changes in glacier maximum displacement and factor of safety.

https://doi.org/10.5194/egusphere-2025-3648
Preprint. Discussion started: 12 December 2025

5. Discussion

Through statistical analysis, there have been 62 recorded IAs on the TP since the 20th century. After the 21st century, the TP shows significant warm and humid characteristics, and the number of IAs has reached more than 20 times (Tang et al., 2024). These IAs are mainly distributed in southeastern Tibet. The glaciers in this area are relatively low in altitude, and most of them belong to temperate glaciers. The stability evaluation and instability mechanism analysis of temperate glaciers are particularly important. The glacier instability mechanisms induced by rising temperature, rainfall and earthquake are described below (Fig. 18).

The rising temperature reduces the temperate glacier stability through melting, lubrication and reduction of ice mechanical properties. The temperature difference causes thermal stress on the glacier surface, which promotes the expansion and deepening of crevasses. Meltwater infiltrates along the crevasses, and the increase of seepage pressure further enhances the crevasses expansion. With glacier ablation and crevasses expansion, the stress concentration area of glaciers is more likely to induce IA. When the meltwater penetrates into the glacier base, a lubricating layer is formed,
resulting in a decrease in friction of the ice-rock interface and an increase in the subglacial water pressure. It makes the glacier accelerate the basal sliding and induce IA. For temperate glaciers, the basal temperature is the melting point, the ice viscosity decreases, and the plastic flow accelerates. Rising temperatures will also reduce the shear and tensile strength of ice, making it more susceptible to crack and collapse within the glacier.

Rainfall can penetrate into the glacier through crevasses, expanding existing crevasses. The rainfall increases the water pressure in the crevasses, causing the crevasses to expand deeper. At the same time, more meltwater generated by rainfall infiltrating into glacier base will also produce a lubrication effect. There are multiple tension cracks at periglacial region, and heavy rainfall will increase the glacier weight, causing slip breaking type IAs at periglacial region.

After the earthquake, the glacier will redistribute internal and external stress. The earthquake can directly induce IAs in a short time. It may also have a lag effect, causing subsequent IAs for a long time. The earthquake will aggravate the expansion and penetration of the glacier crevasses. The liquid water in the crevasses reduces the energy dissipation caused by the seismic wave, and the vibration is easier to

https://doi.org/10.5194/egusphere-2025-3648
Preprint. Discussion started: 12 December 2025

spread to the glacier base. Seismic waves may lead to a sudden increase in the shear force between the glacier and base, and also cause local heat accumulation in the glacier, which induces IAs.

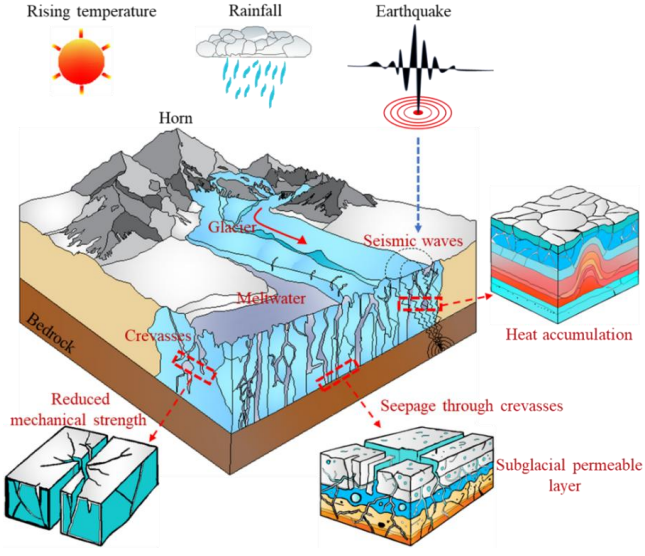

Figure 18. Temperature, rainfall and earthquake induced ice avalanche.

6. Conclusions

Herein, considering the multi-physical factors and their coupling mechanism in the glacier flow process, the dynamic characteristics and hydrothermal distribution of temperate glaciers with climate change were studied, and a conceptual model for quantitative evaluation of the stability and potential collapse area was proposed. The field monitoring and simulation results are compared to verify the reliability of the numerical coupling model and calculation method. The following conclusions were drawn:

(1) The low temperature area is mainly concentrated in the glacier upper reaches. The minimum temperature of the glacier in the cold and warm season can reach -10 and -8℃, respectively. The surface temperature is sensitive to the external environment temperature. The basal temperature is maintained at melting point temperature, and the fluctuation range is not more than 0.25 ℃. The higher the glacier altitude, the greater the fluctuation range of heat flux. The total heat flux in one year is positive, and the time when the heat flux becomes negative is gradually advanced with the increase of years.

https://doi.org/10.5194/egusphere-2025-3648
Preprint. Discussion started: 12 December 2025

(2) The glacier flow velocity in the warm season is significantly greater than that in the cold season. The maximum flow velocity in the cold and warm seasons are 45 and 50 m/yr, respectively. The maximum flow velocity is concentrated in the area with the largest glacier thickness. The mass flow rate of the Midui glacier increases year by year. In the 10th year, the outward mass flow reached 6.13×10^{-2} kg/s.

(3) The abrupt change of displacement, the penetration of plastic strain, and the generalized shear strain are used as the criterion of glacier instability. The glacier instability strip is arc-shaped and located in the upper reaches, where the fluid pressure in the subglacial permeable layer is the highest. In February, the FOS reached a maximum of 2.03. The FOS decreased the most from May to July, and reached the minimum of 1.48 in August./

Data availability. Data will be made available on request.

Author contributions. **Guang Li:** Investigation, Methodology, Software, Formal Analysis, Validation, Writing – original draft, Writing – review and editing. **Minggao Tang:** Conceptualization, Methodology, Data curation, Funding acquisition, Supervision, Resources, Writing – review and editing. **Huanle Zhao:** Investigation, Methodology, Writing – review and editing. **Daojing Guo:** Writing – review and editing. **Xiaonan Yang:** Investigation. **Xu Ran:** Investigation.

Competing interest. The authors declare that they have no conflict of interest.

Acknowledgments. This research has been supported by the National Natural Science Foundation of China (Grant No. 42377199), Chengdu University of Technology Postgraduate Innovative Cultivation Program (Grant No. CDUT2023BJCX008), the Second Tibetan Plateau Scientific Expedition and Research Program (STEP) (Grant No. 2019QZKK0201), and State Key Laboratory of Geohazard Prevention and Geoenvironment Protection Independent Research Project (Grant No. SKLGP2021Z005).

https://doi.org/10.5194/egusphere-2025-3648
Preprint. Discussion started: 12 December 2025

References

Ai, S., Ding, X., An, J., Lin, G., Wang, Z., and Yan, M.: Discovery of the fastest ice flow along the central flow line of Austre Lovénbreen, a poly-thermal valley glacier in Svalbard. Remote Sens. 11(12), 1488. https://doi.org/10.3390/rs11121488, 2019.

Altena, B., Scambos, T., Fahnestock, M., and Kääb, A.: Extracting recent short-term glacier velocity evolution over southern Alaska and the Yukon from a large collection of Landsat data. Cryosphere. 13(3), 795-814. https://doi.org/10.5194/tc-13-795-2019, 2019.

China Meteorological Administration Climate Change Center.: China Climate Change Blue Book (2022), Science Press, Beijing, China, ISBN 978-7-03-072789-3, 2023.

Cook, S., Gillet-Chaulet, F., and Fürst, J.: Robust reconstruction of glacier beds using transient 2D assimilation with Stokes. J. Glaciol. 69(277), 1393-1402. https://doi.org/10.1017/jog.2023.26, 2023.

Dang, C., Chu, N.N., and Zhang, P.: Computing method for discharges of debris flow induced by moraine-dammed lake outburst. J. Glaciol. 41(1), 165-174, 2019.

Faillettaz, J., Funk, M., and Vincent, C.: Avalanching glacier instabilities: Review on processes and early warning perspectives. Rev. Geophys. 53(2), 203-224. https://doi.org/10.1002/2014RG000466, 2015.

Garg, P., Shukla, A., and Jasrotia, A., 2019. On the strongly imbalanced state of glaciers in the Sikkim, eastern Himalaya, India. Sci. Total. Environ. 691, 16-35. https://doi.org/10.1016/j.scitotenv.2019.07.086.

Gilbert, A., Leinss, S., Kargel, J., Kääb, A., Gascoin, S., Leonard, G., Berthier, E., Karki, A., and Yao, T.: Mechanisms leading to the 2016 giant twin glacier collapses, Aru Range, Tibet. Cryosphere. 12(9), 2883-2900. https://doi.org/10.5194/tc-12-2883-2018, 2018.

Gilbert, A., Vincent, C., Gagliardini, O., Krug, J., and Berthier, E.: Assessment of thermal change in cold avalanching glaciers in relation to climate warming. Geophys. Res. Lett. 42(15), 6382-6390. https://doi.org/10.1002/2015GL064838, 2015.

Glen, J.: The creep of polycrystalline ice, Proceedings of the Royal Society of London. Phys Sci 228(1175), 519-538. https://doi.org/10.1098/rspa.1955.0066, 1955.

Gong, Y., Zwinger, T., Cornford, S., Gladstone, R., Schäfer, M., and Moore, J.C.: Importance of basal boundary conditions in transient simulations: case study of a surging marine-terminating glacier on

https://doi.org/10.5194/egusphere-2025-3648
Preprint. Discussion started: 12 December 2025

494 Austfonna, Svalbard. J Glaciol. 63(237), 106-117. https://doi.org/10.1017/jog.2016.121, 2017.
495 Incropera, F., DeWitt, DP., Bergman, TL., Lavine, AS.: Fundamentals of Heat and Mass Transfer 6th
496 Edition, John Wiley & Sons, ISBN 0471457280, 2007.
497 Jacquemart, M., Loso, M., Leopold, M., Welty, E., Berthier, E., Hansen, J.S., Sykes, J., and Ti
498 ampo, K.: What drives large-scale glacier detachments? Insights from Flat Creek glacier, S
499 t. Elias mountains, Alaska. Geology. 48(7), 703-707. https://doi.org/10.1130/G47211.1, 2020.
500 Jisk,oot, H., Fox, T.A., and Van Wychen, W.: Flow and structure in a dendritic glacier with bedrock steps.
501 J Glaciol. 63(241), 912-928. https://doi.org/10.1017/jog.2017.58, 2017.
502 Kääb, A., Jacquemart, M., Gilbert, A., Leinss, S., Girod, L., Huggel, C., Falaschi, D., Ugalde, F., Petrakov,
503 D., Chernomorets, S., and Dokukin, M.: Sudden large-volume detachments of low-angle mountain
504 glaciers–more frequent than thought? Cryosphere. 15(4), 1751-1785. https://doi.org/10.5194/tc-15-
505 1751-2021, 2021.
506 Kääb, A., Leinss, S., Gilbert, A., Bühler, Y., Gascoin, S., Evans, S.G., Bartelt, P., Berthier, E., Brun, F.,
507 Chao, W.A., and Farinotti, D.: Massive collapse of two glaciers in western Tibet in 2016 after surge-
508 like instability. Nat. Geosci. 11(2), 114-120. https://doi.org/10.1038/s41561-017-0039-7, 2018.
509 Karlsson, N.B., Solgaard, A.M., Mankoff, K.D., Gillet-Chaulet, F., MacGregor, J.A., Box, J.E., Citterio,
510 M., Colgan, W.T., Larsen, S.H., Kjeldsen, K.K., and Korsgaard, N.J.: A first constraint on basal
511 melt-water production of the Greenland ice sheet. Nat. Commun. 12(1), 3461.
512 https://doi.org/10.1038/s41467-021-23739-z, 2021.
513 Li, W., Zhao, B., Xu, Q., Scaringi, G., Lu, H., and Huang, R.: More frequent glacier-rock avalanches in
514 Sedongpu gully are blocking the Yarlung Zangbo River in eastern Tibet. Landslides. 1-13.
515 https://doi.org/10.1007/s10346-021-01798-z, 2022.
516 Li, W., Zhao, B., Lu, H., Li, Z., Yu, W., Zhou, S., and Xu, Q.: More mass wasting activities reported in
517 Sedongpu gully of Tibetan Plateau, China. J. Rock. Mech. Geotech. Eng.
518 https://doi.org/10.1016/j.jrmge.2024.07.012, 2024.
519 Li X., Cheng G., Jin H., Kang E., Chei T., Jin R., Wu L., Nan Z., Wang J., and Shen Y.: Cryospheric
520 change in China. Global and Planetary Change, 62(3-4): 210-218.
521 https://doi.org/10.1016/j.gloplacha.2008.02.001, 2008.

https://doi.org/10.5194/egusphere-2025-3648
Preprint. Discussion started: 12 December 2025

522 Millan, R., Mouginot, J., Rabatel, A., and Morlighem, M.: Ice velocity and thickness of the world's
523 glaciers. Nat. Geosci. 15(2), 124-129, 2022.
524 Paranunzio, R. and Marra, F.: Open gridded climate datasets can help investigating the relation
525 between meteorological anomalies and geomorphic hazards in mountainous areas. Global. P
526 lanetary. Change. 232, 104328. https://doi.org/10.1016/j.gloplacha.2023.104328, 2024.
527 Richards, L.: Capillary conduction of liquids through porous mediums. physics. 1(5), 318-333.
528 https://doi.org/10.1063/1.1745010, 1931.
529 Ritz, C.: Time dependent boundary conditions for calculating of temperature fields in ice sheets,
530 International Association of Hydrological Sciences Press, Wallingford, the United States, 1987.
531 Seddik, H., Greve, R., Sakakibara, D., Tsutaki, S., Minowa, M., and Sugiyama, S.: Response o
532 f the flow dynamics of Bowdoin Glacier, northwestern Greenland, to basal lubrication and
533 tidal forcing. J. Glaciol. 65(250), 225-238. https://doi.org/10.1017/jog.2018.106, 2019.
534 Stocker T.: The Physical Science Basis, Contribution of Working Group I to the Fifth Assessment Report
535 of the Intergovernmental Panel on Climate Change, Cambridge University Press, Cambridge,
536 England, 2013.
537 Tang, M., Li, G., Zhao, H., Xu, Q., Wu, G., Yang, W., and Guo, D.: Advances in ice avalanc
538 hes on the Tibetan Plateau. J. Mountain. Sci. 21(6), 1814-1829. https://doi.org/10.1007/s116
539 29-023-8530-7, 2024.
540 Tang, M., Liu, X., Li, G., Zhao, H., Xu, Q., Zhu, X., and Li, W.: Mechanism of ice avalanche in the
541 Sedongpu sag, Yarlung Zangbo River basin-an experimental study. Earth. Sci. Front. 30(4), 405,
542 2023.
543 Tannehill, J.C., Anderson, D.A., and Pletcher, R.H.: Computational fluid mechanics and heat tra
544 nsfer. In: Series in Computational and Physical Processes in Mechanics and Thermal Scien
545 ces. Taylor. Francis. Pub. https://doi.org/10.1201/9781351124027, 1997.
546 Vallot, D., Pettersson, R., Luckman, A., Benn, D.I., Zwinger, T., Van Pelt, W.J., Kohler, J., Schäfer, M.,
547 Claremar, B., and Hulton, N.R.: Basal dynamics of Kronebreen, a fast-flowing tidewater glacier in
548 Svalbard: non-local spatio-temporal response to water input. J. Glaciol. 63(242), 1012-1024.
549 https://doi.org/10.1017/jog.2017.69, 2017.

https://doi.org/10.5194/egusphere-2025-3648
Preprint. Discussion started: 12 December 2025

Van Genuchten, M.T.: A closed‐form equation for predicting the hydraulic conductivity of unsaturated soils. Soil. Sci. Soc. Am. J, 44(5), 892-898. https://doi.org/10.2136/sssaj1980.03615995004400050002x, 1980.

Wagner, W., Saul, A., and Pruss, A.: International equations for the pressure along the melting and along the sublimation curve of ordinary water substance. J. Phys. Chemi. Ref. Data, 23(3), 515-527. https://doi.org/10.1063/1.555947, 1994.

Wang. N., Yao. T., Xu. B., Chen, A., and Wang, W.: Spatiotemporal pattern, trend, and influen ce of glacier change in Tibetan Plateau and surroundings under global warming. Bullet. C hinese. Academy. Sci. 34(11), 1220-1232. https://doi.org/10.16418/j.issn.1000-3045.2019.11.0 05, 2019.

Wang, Y., Zhang, T., Ren, J., Qin, X., Liu, Y., Sun, W., Chen, J., Ding, M., Du, W., and Qin, D.: An investigation of the thermomechanical features of Laohugou Glacier No. 12 on Qilian Shan, western China, using a two-dimensional first-order flow-band ice flow model. Cryosphere. 12(3), 851-866. https://doi.org/10.5194/tc-12-851-2018, 2018.

Wei, M., Zhang, L., and Jiang, R.: A conceptual model for evaluating the stability of high-altit ude ice-rich slopes through coupled thermo-hydro-mechanical simulation. Eng. Geol. 334, 1 07514. https://doi.org/10.1016/j.enggeo.2024.107514, 2024.

Zhang, T., Wang, W., Shen, Z., Zhan, N., Wang, Z., and An, B.: Understanding the 2004 glaci er detachment in the Amney Machen Mountains, northeastern Tibetan Plateau, via multi-ph ase modeling. Landslides. 20(2), 315-330. https://doi.org/10.1007/s10346-022-01989-2, 2023 a.

Zhang, T., Xiao, C., Colgan, W., Qin, X., Du, W., Sun, W., Liu, Y., and Ding, M.: Observed and modelled ice temperature and velocity along the main flowline of East Rongbuk Glacier, Qomolangma (Mount Everest), Hima. J. Glaciol. 59(215), 438-448. https://doi.org/10.3189/2013JoG12J202, 2013.

Zhang, T., Yin, Y., Li, B., Liu, X., Wang, M., Gao, Y., Wan, J., and Gnyawali, K.R.: Characte ristics and dynamic analysis of the February 2021 long-runout disaster chain triggered by massive rock and ice avalanche at Chamoli, Indian Himalaya. J. Rock. Mechan. Geotech.

https://doi.org/10.5194/egusphere-2025-3648
Preprint. Discussion started: 12 December 2025

578 Eng. 15(2), 296-308. https://doi.org/10.1016/j.jrmge.2022.04.003, 2023b.
579 Zhao, L., Tian, L., Zwinger, T., Ding, R., Zong, J., Ye, Q., and Moore, J.C.: Numerical simula
580 tions of Gurenhekou Glacier on the Tibetan Plateau using a full-Stokes ice dynamical m
581 odel. Cryosphere. Discuss. 7(1), 145-173. https://doi.org/10.5194/tcd-7-145-2013, 2013.
582 Zhao, W., Zhao, L., Tian, L., Wolovick, M., and Moore, J.C.: Simulating the evolution of Da Anglong
583 Glacier, western Tibetan Plateau over the 21st century. Water. 14(2), 271.
584 https://doi.org/10.3390/w14020271, 2022.
585 Zhen, W., Shiyin, L., and Xiaobo, H.: Numerical simulation of the flow velocity and temperature of the
586 Dongkemadi Glacier. Environ. Earth. Sci. 75, 1-11. https://doi.org/10.1007/s12665-016-5262-9,
587 2016.
588 Zou, C., Jansen, J.D., Carling, P.A., Dou, X., Wei, Z., and Fan, X.: Triggers for multiple glaci
589 er detachments from a low-angle valley glacier in the Amney Machen Range, eastern Tibe
590 tan Plateau. Geomorphol. 440, 108867. https://doi.org/10.1016/j.geomorph.2023.108867, 202
591 3.